available at www.sciencedirect.com

ScienceDirect

www.elsevier.com/locate/brainres

BRAIN RESEARCH

Research Report

# Brain and retinal ferroportin 1 dysregulation in polycythaemia mice

*Jared Iacovelli*[a], *Agnieska E. Mlodnicka*[b], *Peter Veldman*[a], *Gui-Shuang Ying*[a], *Joshua L. Dunaief*[a,*], *Armin Schumacher*[b]

[a]*F. M. Kirby Center for Molecular Ophthalmology, Scheie Eye Institute, University of Pennsylvania, 305 Stellar-Chance Labs, 422 Curie Blvd, Philadelphia, PA 19104, USA*

[b]*Department of Molecular and Human Genetics, Baylor College of Medicin, Houston, Texas, USA*

ARTICLE INFO

*Article history:*
Accepted 26 June 2009
Available online 9 July 2009

*Keywords:*
Polycythaemia
Ferroportin
Brain
Retina
Iron

ABSTRACT

Disruption of iron homeostasis within the central nervous system (CNS) can lead to profound abnormalities during both development and aging in mammals. The radiation-induced polycythaemia (Pcm) mutation, a 58-bp microdeletion in the promoter region of ferroportin 1 (Fpn1), disrupts transcriptional and post-transcriptional regulation of this pivotal iron transporter. This regulatory mutation induces dynamic alterations in peripheral iron homeostasis such that newborn homozygous *Pcm* mice exhibit iron deficiency anemia with increased duodenal Fpn1 expression while adult homozygotes display decreased Fpn1 expression and anemia despite organismal iron overload. Herein we report the impact of the Pcm microdeletion on iron homeostasis in two compartments of the central nervous system: brain and retina. At birth, *Pcm* homozygotes show a marked decrease in brain iron content and reduced levels of Fpn1 expression. Upregulation of transferrin receptor 1 (TfR1) in brain microvasculature appears to mediate the compensatory iron uptake during postnatal development and iron content in Pcm brain is restored to wild-type levels by 7 weeks of age. Similarly, changes in expression are transient and expression of Fpn1 and TfR1 is indistinguishable between *Pcm* homozygotes and wild-type by 12 weeks of age. Strikingly, the adult *Pcm* brain is effectively protected from the peripheral iron overload and maintains normal iron content. In contrast to Fpn1 downregulation in perinatal brain, the retina of *Pcm* homozygotes reveals increased levels of Fpn1 expression. While retinal morphology appears normal at birth and during early postnatal development, adult *Pcm* mice demonstrate a marked, age-dependent loss of photoreceptors. This phenotype demonstrates the importance of iron homeostasis in retinal health.



## 1. Introduction

Iron functions as an essential co-factor for heme and multiple non-heme proteins (Hentze et al., 2004). In addition to meeting a physiological demand, tight regulation of cellular and organismal iron levels also prevents the untoward oxidation–reduction chemistry of iron overload (Aisen et al., 2001). While recent years have witnessed significant progress in elucidating the mechanisms of peripheral iron homeostasis in mammals, the regulation of iron balance in the central

* *Corresponding author*. Fax: +1 215 573 8083.
E-mail address: jdunaief@mail.med.upenn.edu (J.L. Dunaief).

0006-8993/$ – see front matter © 2009 Elsevier B.V. All rights reserved.
doi:10.1016/j.brainres.2009.06.098

nervous system (CNS) remains poorly understood. Iron-dependent processes in the CNS include regulation of the amount and composition of myelin (Kwik-Uribe et al., 2000), synthesis and degradation of neurotransmitters by enzymes such as tryptophan hydroxylase and tyrosine hydroxylase (Yehuda and Youdim, 1989), and control of GABAergic activity (Taneja et al., 1986). Insights gleaned from both dietary manipulation and hereditary disorders underscore the critical role of iron and iron-related genes in brain function (Beard, 2003; Ponka, 2004). Early stages of neurodevelopment in humans and various model organisms appear particularly vulnerable to iron deficiency and, despite subsequent repletion of CNS iron balance, behavioral and biochemical abnormalities can manifest at later stages of life (Beard, 2003; Beard, 2007; Beard and Connor, 2003).

Beyond development, recent studies also implicated abnormal iron homeostasis in neurodegeneration. For example, patients with neuroferritinopathy, Friedreich's Ataxia, panthothenate kinase-associated neurodegeneration (PKAN) or aceruloplasminemia manifest iron deposits in various regions of the CNS and have severe neurological abnormalities, including extrapyramidal dysfunction or cerebellar ataxia (Curtis et al., 2001; Pandolfo, 1999; Xu et al., 2004; Zhou et al., 2001). Likewise, loss of function of the ferroxidase ceruloplasmin (Cp), which is required for iron efflux from astrocytes (Jeong and David, 2003), revealed iron accumulation in murine CNS (Jeong and David, 2006; Patel et al., 2002). Severe defects in brain iron homeostasis and degenerative movement disorder were reported for targeted disruption of Iron regulatory protein 2 (LaVaute et al., 2001).

Aside from brain and spinal cord, the retina represents another CNS region with increased susceptibility to iron overload-induced degenerative sequelae. Using Perls' histochemistry to detect iron, elevated iron levels were detected in *post mortem* retinas from age-related macular degeneration (AMD) donors compared to healthy age-matched controls (Hahn et al., 2003). In addition, a case of AMD with geographic atrophy had increased immunolabeling for ferritin and ferroportin 1 compared to an age-matched control (Dentchev et al., 2005). Occurrences of retinal abnormalities have also been reported in patients with PKAN, Friedreich's Ataxia, and Hereditary Hemochromatosis (He et al., 2007). Maculopathy has been demonstrated in patients with aceruloplasminemia, who accumulate iron by their fifth or sixth decade of life in retina and others tissues (Dunaief et al., 2005; Miyajima et al., 1987; Morita et al., 1995; Yamaguchi et al., 1998). Similarly, mice deficient for *Cp* and its homolog *Heph* (Hephaestin) had morphologic features reminiscent of AMD, including retinal iron accumulation, pigment epithelium hypertrophy, hyperplasia and death, photoreceptor degeneration and subretinal neovascularization (Hadziahmetovic et al., 2008; Hahn et al., 2004).

The ferroxidases Cp and Heph oxidize iron from the ferrous ($Fe^{2+}$) to the ferric form ($Fe^{3+}$) in support of cellular iron export by ferroportin 1 (Fpn1). Based on the functional cooperation between ferroxidases and Fpn1 in the regulation of iron efflux, it is expected that disruption of Fpn1 activity would cause aberrant iron homeostasis in the CNS, including retina. The present study tests this hypothesis in polycythaemia (*Pcm*) mice, which carry a radiation-induced 58-bp microdeletion in the Fpn1 promoter region (Mok et al., 2004a). The polycythaemia mutation is characterized by an erythropoietin-dependent increase in red blood cells in heterozygotes and a hypochromic, microcytic anemia in homozygotes. This regulatory mutation causes tissue-specific dysregulation of Fpn1 expression and results in the gamut of systemic iron homeostasis defects, ranging from iron deficiency at birth to tissue iron overload in adult *Pcm* mice (Mok et al., 2004a,b, 2006).

Our results show perinatal iron deficiency in *Pcm* homozygous brain, which returns to normal iron levels by 7 weeks of age. Immunohistochemistry reveals a striking decrease in Fpn1 expression in smooth muscle cells of meningeal arterioles and endothelial cells of interstitial capillaries at birth, suggesting decreased iron import into the brain of *Pcm* homozygotes during development. Compensatory upregulation of transferrin receptor 1 (TfR1) expression in brain microvasculature appears to mediate the recovery from perinatal iron deficiency. In contrast, across the layers of the perinatal retina *Pcm* homozygotes demonstrate increased Fpn1 and TfR1 expression followed by an age-related degeneration of photoreceptors. Our results demonstrate that dysregulation on *Fpn1* expression perturbs developmental brain iron homeostasis and leads to retinal degeneration, which is consistent with the importance of iron homeostasis in CNS health.

## 2. Results

### 2.1. *Severe developmental iron deficiency recovers to normal iron balance in adult Pcm brain*

In the context of an embryonic iron deficiency (Mok et al., 2004a,b), *Pcm* pups demonstrated a profound decrease in brain iron content at P0 (Fig. 1A). Notably, *Pcm* heterozygotes and homozygotes contained only approximately 70% and 25%, respectively, of wild-type brain iron levels. At 3 weeks, the iron content of *Pcm* brain approximated 85% of wild-type, reflecting compensatory iron uptake during early postnatal development (Fig. 1A). However, iron balance in *Pcm* brain remained significantly lower compared with wild-type, indicating a protracted recovery from the severe developmental iron deficiency. In contrast to the marked iron accumulation in visceral organs (Mok et al., 2004a), the iron content in 7- and 12-week-old *Pcm* brain was indistinguishable from wild-type (Fig. 1A). Furthermore, Perls' Prussian Blue staining on *Pcm* brain sections did not reveal evidence of localized iron accumulation (data not shown). This comports with normal brain iron content in aged cohorts of *Pcm* homozygotes and wild-type littermates (Mok et al., 2006). Thus, whereas both peripheral tissues and brain displayed severe iron deficiency developmentally, adult brain appeared protected from the systemic iron overload.

### 2.2. *The Pcm microdeletion causes a transient decrease in Fpn1 expression in the developing brain*

Previous studies in *Pcm* mice detected tissue- and stage-specific dysregulation of Fpn1 expression (Mok et al., 2004a,b, 2006). In order to assess the effects of the *Pcm* microdeletion

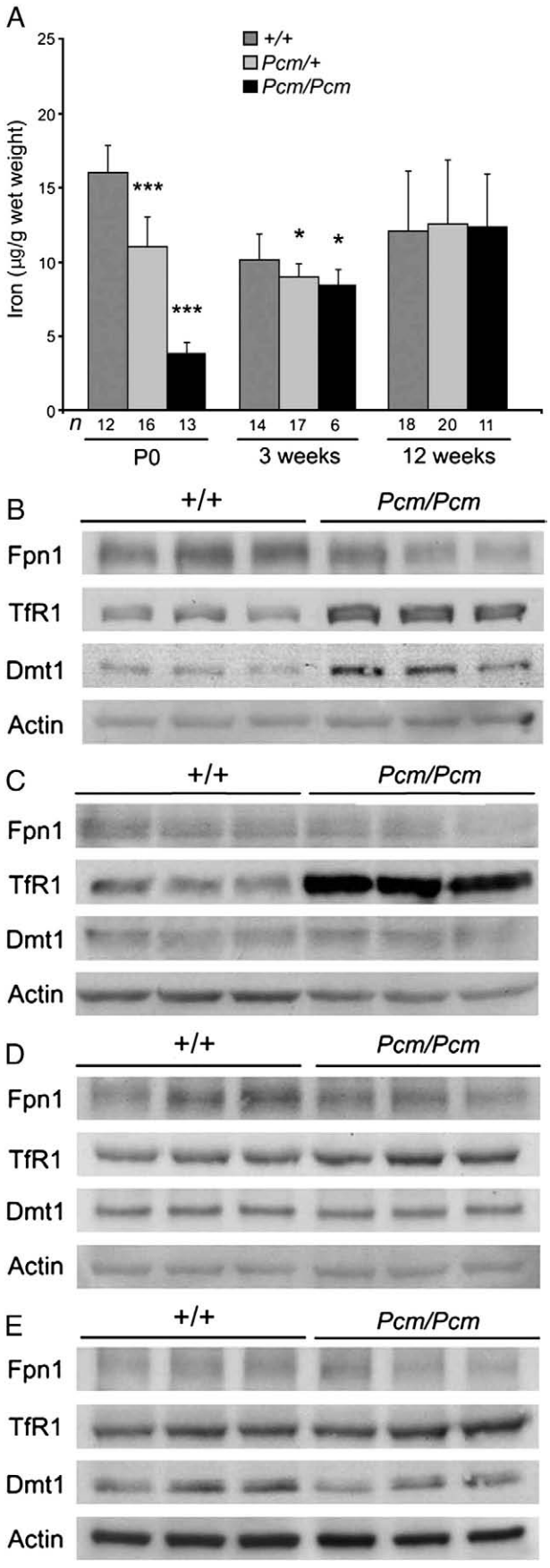


on Fpn1 expression in the developing brain, Western blot analysis was performed on lysates from wild-type and *Pcm* mutants between E14.5 and 12 weeks of age. *Pcm* homozygous brain manifested a decrease in Fpn1 levels between E14.5 and 3 weeks (Figs. 1B–D). By 12 weeks of age, Fpn1 expression recovered to wild-type levels (Fig. 1E). Quantitative real-time PCR revealed a significant decrease in *Fpn1* mRNA expression in *Pcm* homozygous brain compared to wild-type at P0. In contrast, at 12 weeks of age, wild-type and *Pcm* homozygous brains had similar *Fpn1* mRNA expression levels (Fig. 2). Thus, similar to placenta and fetal liver (Mok et al., 2004b), concordance between *Fpn1* transcript and protein levels implicated transcriptional downregulation of Fpn1 expression as the primary molecular defect caused by the *Pcm* microdeletion in the developing brain.

By immunohistochemistry, P0 and 3-week-old *Pcm* brain exhibited significantly decreased Fpn1 expression in smooth muscle cells of meningeal arterioles, as well as in endothelial cells of interstitial capillaries (Figs. 3A, A′, D, D′). There was no detectable difference in Fpn1 expression between wild-type and *Pcm* vessels at 12 weeks of age (Figs. 3G, G′). Fpn1 expression in other cell types, including neurons, glia, choroid plexus and ependymal cells, appeared unaffected by the *Pcm* mutation (Figs. 3A, A′, D, D′G, G′ and data not shown). Since Fpn1 is considered a likely candidate for iron transport across the abluminal membrane of endothelial cells at the blood–brain barrier (Ponka, 2004; Wu et al., 2004), decreased Fpn1-mediated iron transport into the brain could compound the embryonic systemic iron deficiency, resulting in markedly decreased brain iron levels at P0 (Figs. 1A, A′).

### 2.3. *Compensatory expression of iron transport proteins in the developing Pcm brain*

Normal iron balance in adult *Pcm* brain (Fig. 1A) implicated compensatory mechanism(s) in the recovery from developmental iron deficiency. Furthermore, adult *Pcm* brain appeared

**Fig. 1 – Brain iron content and expression of iron transport proteins. (A) Compared with wild-type littermates, *Pcm* mutant brain demonstrated a significant decrease in non-heme iron content at P0, more severe in homozygotes. Asterisks, $P < 0.0001$. At three weeks of age, brain iron content in *Pcm* mutants remained significantly lower compared with wild-type littermates. Asterisk, $P < 0.05$. All genotypes exhibited similar brain iron balance at 12 weeks of age. The number (*n*) of brains analyzed per genotype is shown at the bottom of the diagram. Error bars indicate s.d.. (B–E) Western blot analysis of iron transport proteins in E14.5 (B), P0 (C), 3-week (D) and 12-week-old brain (E). At E14.5 and P0, *Pcm* homozygotes exhibited a moderate decrease in Fpn1 expression and marked upregulation of TfR1 and Dmt1. While TfR1 levels remained discretely elevated at 3 weeks of age, Fpn1 and Dmt1 expression was indistinguishable between wild-type and *Pcm* homozygotes. In contrast, at 12 weeks of age, Dmt1 expression appeared decreased in the context of normal Fpn1 and TfR1 levels. Approximate molecular weight masses: Fpn1 68 kDa, TfR1 95 kDa, Dmt1 63 kDa, and actin 41 kDa.**

protected from the peripheral iron overload (Fig. 1A), which resulted from increased duodenal uptake during postnatal development (Mok et al., 2004a, 2006). Towards elucidation of the underlying regulatory mechanisms, Western blot analysis identified stage-specific changes in the expression of iron transporters. For example, E14.5 and P0 brain from *Pcm* mutants displayed elevated expression of TfR1 and divalent metal transporter 1 (Dmt1) (Figs. 1B, C). While Dmt1 expression recovered to wild-type levels in 3-week-old *Pcm* homozygotes, TfR1 levels remained elevated (Fig. 1D). At 12 weeks of age, TfR1 expression was indistinguishable between wild-type and *Pcm* brain (Fig. 1E). Interestingly, Dmt1 levels were significantly lower at this stage, suggesting a potential role for Dmt1 in the protection from brain iron overload.

Quantitative real-time PCR demonstrated a statistically significant increase in *TfR1* mRNA levels in *Pcm* homozygous brain at P0 (Fig. 2). This is consistent with increased stabilization of *TfR1* mRNA due to binding of iron regulatory proteins in response to cellular iron deficiency (Hentze et al., 2004). *TfR1* mRNA levels remained elevated at 12 weeks of age (Fig. 2). The significance of this finding in the context of normal brain iron content is unknown. *Dmt1* mRNA levels were indistinguishable between *Pcm* homozygous and wild-type brain at both P0 and 12 weeks of age (Fig. 2), suggesting a predominantly post-transcriptional mechanism of *Dmt1* regulation in response to brain iron content. Likewise, transcript levels of other iron metabolism genes, including Trf and Hepcidin (Hamp), were normal in P0 and 12-week-old *Pcm* homozygotes (Fig. 2).

Fpn1, TfR1 and Dmt1 protein expression was dynamically regulated in *Pcm* brain vessels. For example, immunohistochemistry showed marked upregulation of TfR1 expression in *Pcm* brain vessels during early postnatal development, which gradually decreased to wild-type levels by 12 weeks of age (Figs. 3B, B′E, E′, H, H′). While *Pcm* vessels exhibited discrete upregulation of Dmt1 at P0, expression levels at 3 weeks of age were comparable to wild-type littermates (Figs. 3C, C′, F, F′). Consistent with Western blot analysis, a subtle but reproducible decrease in Dmt1 expression was detected in *Pcm* vessels compared with wild-type at 12 weeks of age (Figs. 3I, I′).

Beyond differences in temporal regulation, compensatory changes in TfR1 and Dmt1 expression encompassed distinct subsets of brain vessels. Whereas upregulation of TfR1 in P0 and 3-week-old *Pcm* brain was confined to endothelial cells of small interstitial vessels (Figs. 3B, B′, E, E′), Dmt1 expression was dynamically regulated in endothelial and smooth muscle cells of larger meningeal vessels (Figs. 3C, C′, E, E′). There was no evidence for significant changes in expression of both iron transporters in other cell types (Fig. 3, and data not shown). These findings conform to the notion that the vasculature represents a pivotal site for dynamic regulation of iron transporter expression in response to brain iron content (Rouault, 2001). In addition, they strongly suggest that compensatory mechanisms are operational at early stages of brain development, potentially ameliorating the developmental iron deficiency in *Pcm* mutants.

### 2.4. *Increased Fpn1 protein level in the perinatal Pcm retina is associated with an age-related degeneration of the photoreceptors*

Deficiency in the ferroxidases Cp and Heph, which along with Fpn1 function to export iron from cells, leads to an age-related

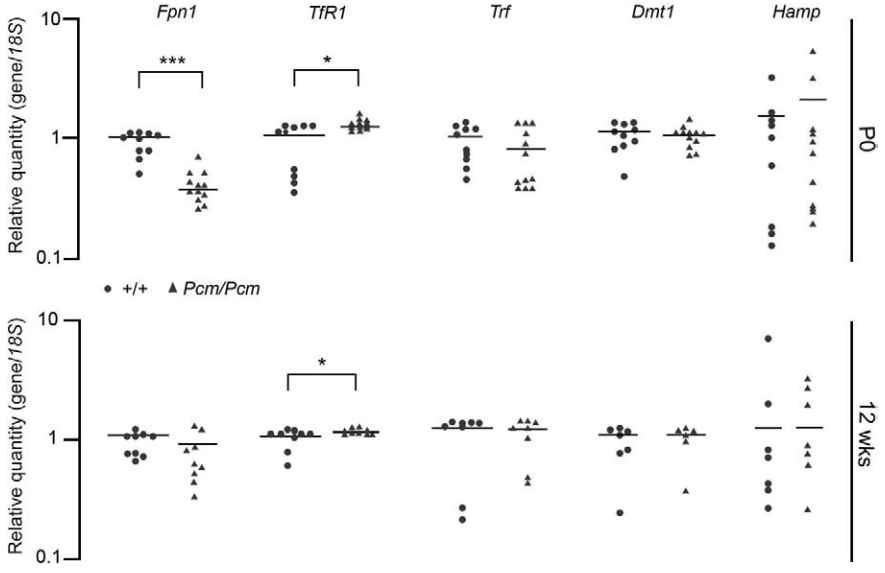


**Fig. 2 – mRNA levels of iron metabolism genes in *Pcm* brain. mRNA expression levels of several iron metabolism genes in P0 and 12-week-old brain were evaluated by quantitative real-time RT-PCR using *18S* ribosomal RNA as an endogenous control. The *N* was at least 3 for all comparisons. The relative amounts of *Fpn1*, *TfR1*, *Trf*, *Dmt1* or *Hamp* mRNA levels were expressed as the ratio of the gene-specific probe to *18S* ribosomal RNA, and normalized to a single wild-type ratio set to 1. Note statistically significant differences in *Fpn1* (asterisks, $P<0.0001$) and *TfR1* transcript levels (asterisk, $P<0.05$) at P0, as well as in TfR1 levels (asterisk, $P<0.05$) at 12 weeks of age. All other comparisons were not statistically different between genotypes. Horizontal bars indicate the mean of mRNA levels per transcript and genotype. Transcripts and stages of brain development are listed above and to the right of the diagrams, respectively. The key in the center of the diagram depicts the symbols for wild-type and *Pcm* homozygous animals.**

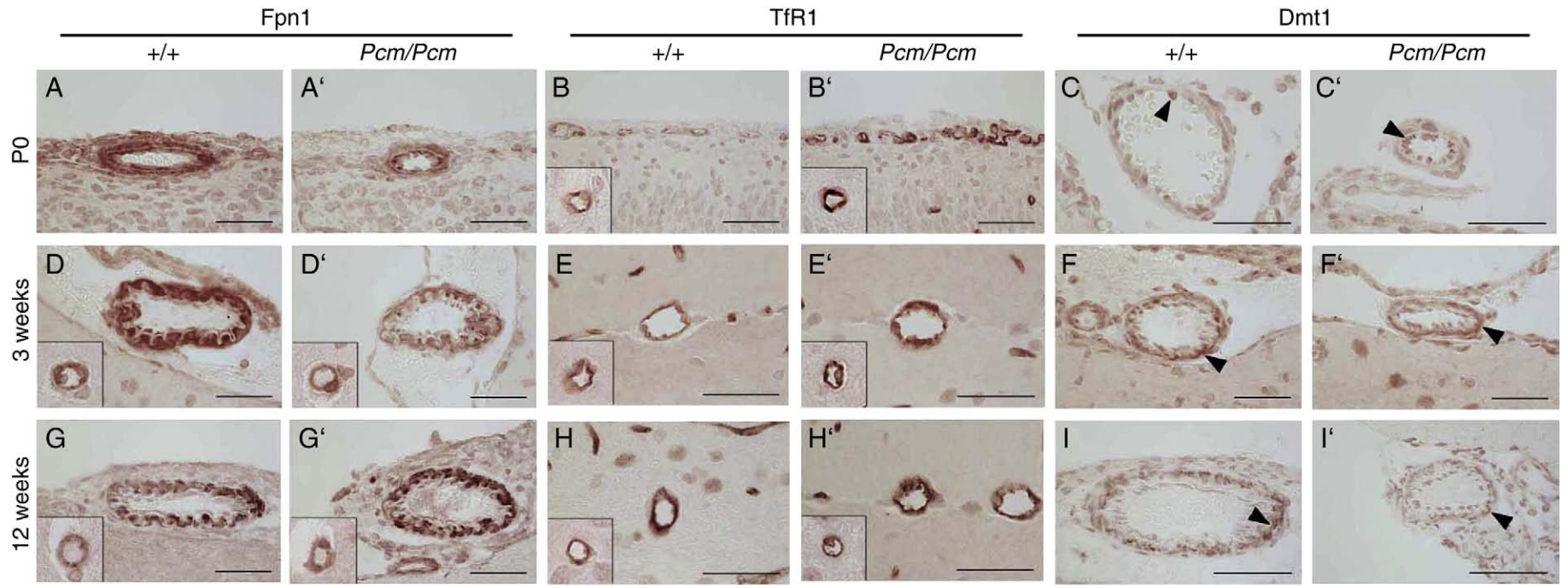


**Fig. 3 – Expression of iron transport proteins in *Pcm* brain. Between P0 and 12 weeks of age, immunohistochemistry detected dynamic changes in Fpn1, TfR1, and Dmt1 expression in *Pcm* brain vessels. For accurate comparison of expression levels, sections from wild-type and *Pcm* homozygous brain were mounted side by side on the same slide. Images depict expression of iron transport proteins in meningeal arterioles, except for panels E, E′, H, and H′, which show larger interstitial vessels. All insets reveal expression in interstitial capillaries. *Pcm* homozygotes demonstrated decreased levels of Fpn1 expression in smooth muscle cells of meningeal arterioles, as well as in endothelial cells of interstitial capillaries at P0 and 3 weeks of age (A,A′,D,D′). This contrasts with marked upregulation of TfR1 in endothelial cells of interstitial capillaries in *Pcm* homozygotes (B,B′,E,E′). Changes in Dmt1 expression were rather discrete and *Pcm* homozygotes displayed a modest increase in Dmt1 levels at P0 (C,C′). In contrast, at 12 weeks of age, Dmt1 levels were reproducibly reduced in *Pcm* homozygotes (I,I′). Note punctate Dmt1 expression in endothelial cells of meningeal arterioles at P0 and larger domains of expression in smooth muscle cells at 3- and 12-weeks of age (arrowheads). Genotypes and iron transporter expression detected by immunohistochemistry are indicated above representative images. The stages of brain development are shown to the left of the panels. Scale bar in all images: 0.04 mm. The width of all insets represents 0.026 mm.**

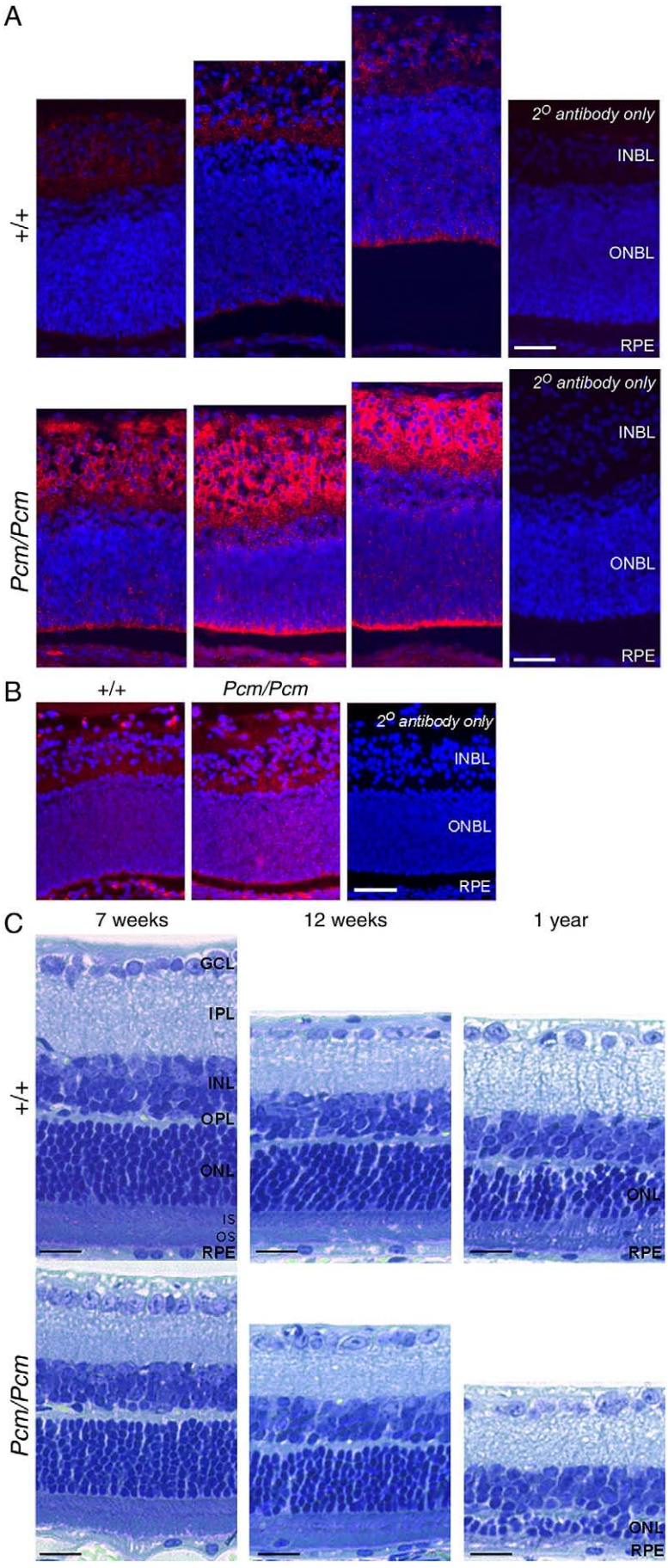
A
+/+
2O antibody only
INBL
ONBL
RPE
Pcm/Pcm
2O antibody only
INBL
ONBL
RPE
B
+/+
Pcm/Pcm
2O antibody only
INBL
ONBL
RPE
C
7 weeks
12 weeks
1 year
+/+
GCL
IPL
INL
OPL
ONL
IS
OS
RPE
ONL
RPE
Pcm/Pcm
ONL
RPE

retinal degeneration (Hadziahmetovic et al., 2008; Hahn et al., 2004). Therefore, we investigated whether dysregulation of *Fpn1* in *Pcm* homozygotes may affect retinal morphology and expression of pivotal iron metabolism genes. Compared to wild-type littermates, the retinas from P0 *Pcm* mice displayed stronger Fpn1 immunolabeling throughout the inner neuroblastic layer (INBL) and the rudimentary photoreceptor inner segments (Fig. 4A). A slight increase was also observed in the retinal pigment epithelium (RPE). Increased TfR1 immunolabel was found in the outer neuroblastic layer (ONBL) and the rudimentary photoreceptor inner segments of retinas from P0 *Pcm* mice when compared to wild-type controls. L-ferritin and H-ferritin expression were comparable between wild-type and *Pcm* retinas at P0 (data not shown).

Dysregulation of Fpn1 in P0 retina suggested the possibility of abnormalities in retinal development. However, at 7 weeks of age, the number of photoreceptor nuclei (within the outer nuclear layer; ONL) was indistinguishable between wild-type and *Pcm* homozygotes (8.59+/−0.10 nuclei per row vs. 9.01+/−0.61 respectively, $P=0.51$; Fig. 4B, Table 1). Additionally, the inner nuclear layer (INL), inner plexiform layer (IPL), and ganglion cell layer (GCL) appeared morphologically normal. Quantification of iron levels from 7 week wild-type and *Pcm* homozygotes retinas (0.058+/−0.004 μg/retina vs. 0.069+/−0.001 μg/retina, $P=0.1402$) and RPE/choroids (0.0065+/−0.008 μg/RPE/choroid vs. 0.060+/−0.001 μg/RPE/choroid, $P=0.6688$) no difference. Furthermore, at 7 weeks of age, Western blot analysis and immunofluorescence revealed no significant difference in Fpn1, TfR1, or L-ferritin levels between wild-type and Pcm homozygous retinas (data not shown). Strikingly, upon aging, the ONL became progressively thinner and at 12 weeks of age counts were trending close to statistical significance (Table 1). At 1 year of age, the number of photoreceptor nuclei per row was significantly lower in *Pcm* retina (2.21+/−0.20) compared with wild-type (5.01+/−0.30, $P=0.02$; Fig. 5B, Table 1). Furthermore, photoreceptor inner and outer segments were absent from most areas of *Pcm* retina by 1 year. Thus, Pcm homozygotes demonstrated an age-dependent, progressive retinal degeneration.

## 3. Discussion

Previous studies have demonstrated that the *Pcm* mutation manifests different cellular and molecular alterations based on the age of the animal and the tissue studied (Mok et al., 2004a,b, 2006). In the context of decreased placental Fpn1 protein levels, *Pcm* homozygotes display systemic iron deficiency and anemia at birth. During early postnatal development elevated duodenal Fpn1 expression governs increased organismal iron uptake. Concomitant low hepcidin levels, hence, an ineffective Fpn1-hepcidin homeostatic loop (Nemeth et al., 2004), result in marked organismal iron uptake and abnormally high iron levels in peripheral tissues, including liver, kidney, duodenum, and heart, reminiscent of patients with ferroportin disease (also known as hereditary hemochromatosis, type IV) (Mok et al., 2004a,b, 2006).

These findings raise the question as to how two components of the CNS, the brain and the retina, respond to the dynamic changes in peripheral iron balance in Pcm mutants. Although parallels between iron homeostasis in the CNS and peripheral tissues have been noted, the blood–brain barrier (BBB) and the blood–cerebrospinal barrier effectively compartmentalize the CNS and necessitate controlled transport of molecules and ions, including iron (Ballabh et al., 2004; Bradbury, 1997). Fpn1 is considered a likely candidate for iron transport across the abluminal membrane of endothelial cells at the BBB (Ponka, 2004).

*Pcm* homozygotes demonstrated decreased levels of Fpn1 expression in smooth muscle cells of meningeal arterioles, as well as in endothelial cells of interstitial capillaries at P0 and 3 weeks of age (Fig. 3). Reduced levels of Fpn1 expression in cerebral blood vessels could compound the developmental brain iron deficiency by decreasing iron flux across the BBB resulting in markedly decreased brain iron levels at P0 (Fig. 1A). Pcm brain iron balance recovered to wild-type levels by 7 weeks of age, presumably due to compensatory increases in iron transport across the BBB. Indeed, *Pcm* brain at E14.5 and P0 displayed elevated expression of TfR1 and Dmt1 (Figs. 1B, C, 2, and 3). However, whereas Dmt1 expression returned to wild-type levels at 3 weeks of age, TfR1 expression remained elevated in *Pcm* homozygous brain, most notably in capillary endothelial cells (Fig. 3). These results are consistent with a pivotal role for TfR1 and, to a lesser extent, Dmt1 compensatory brain iron uptake (Moos and Morgan, 2000; Rouault, 2001; Taylor et al., 1991).

Importantly, brain iron content at 7 and 12 weeks of age was indistinguishable between wild-type and Pcm mutant mice. This indicates the presence of effective mechanisms to protect the *Pcm* brain from sustained peripheral iron overload. Intact compartmentalization of the CNS iron cycle was reminiscent of normal brain iron balance in humans with secondary iron overload (Ponka, 2004). Iron accumulation in

**Fig. 4 – Perinatal increase in Fpn1 and TfR1 immunolabel in *Pcm* retina and age-related degeneration. (A) Fluorescence photomicrographs of P0 retina from wild-type (+/+) and *Pcm* homozygote mice (*Pcm/Pcm*). Sections were labeled in parallel with rabbit anti-Fpn1 and a Cy3-conjugated secondary antibody and images were captured using equivalent exposures. Sections from 3 mice for each genotype are shown. Fpn immunolabel is increased in the INBL and the developing photoreceptor inner segments of *Pcm* retinas compare to wild-type. Scale bar is 50 μm. (B) Fluorescence photomicrographs of P0 retina from wild-type (+/+) and *Pcm* homozygote mice (*Pcm/Pcm*). Sections were labeled in parallel with rabbit anti-TfR1 and a Cy3-conjugated secondary antibody and images were captured using equivalent exposures. Representative sections for each genotype are shown. TfR1 immunolabel is increased in the ONBL and the developing photoreceptor inner segments of *Pcm* retinas compare to wild-type. Scale bar is 50 μm. (C) Light photomicrographs of Toluidine Blue stained plastic sections. The age-dependent retinal degeneration in A/J retinas is more pronounced in *Pcm* homozygotes than in wild-types. By 1 year the outer nuclear layer (ONL) in *Pcm* retina is reduced to 1–3 photoreceptor nuclei per row and inner (IS) and outer segements (OS) are mostly absent. Images are 400 μm from the edge of the optic nerve head. Scale bar is 20 μm.**

**Table 1 – Comparison of photoreceptor nuclei number between wild-type and *Pcm/Pcm* retinas.**

| | Distance | Wild-type Mean (SE) | Mutant type Mean (SE) | P-value [a] |
|---|---|---|---|---|
| Age 7 wks | 200 | 8.28 (0.31) | 8.19 (0.66) | 0.90 |
| | 300 | 8.54 (0.13) | 9.21 (0.78) | 0.42 |
| | 400 | 8.74 (0.02) | 9.31 (0.54) | 0.34 |
| | 500 | 8.78 (0.09) | 9.34 (0.53) | 0.33 |
| | Overall | 8.59 (0.10) | 9.01 (0.61) | 0.51 |
| Age 12 wks | 200 | 8.08 (0.40) | 6.55 (0.22) | 0.08 |
| | 300 | 8.76 (0.40) | 6.95 (0.27) | 0.07 |
| | 400 | 8.42 (0.17) | 7.02 (0.11) | 0.047 |
| | 500 | 8.59 (0.30) | 7.08 (0.20) | 0.06 |
| | Overall | 8.46 (0.29) | 6.90 (0.20) | 0.06 |
| Age 1 yr | 200 | 4.67 (0.41) | 2.17 (0.25) | 0.03 |
| | 300 | 5.00 (0.32) | 2.21 (0.20) | 0.02 |
| | 400 | 5.14 (0.31) | 2.17 (0.21) | 0.02 |
| | 500 | 5.23 (0.16) | 2.28 (0.18) | 0.02 |
| | Overall | 5.01 (0.30) | 2.21 (0.20) | 0.02 |

Quantification of the number of photoreceptor nuclei present in the ONL at a given distance from the edge of the optic nerve head. $N = 3$ eyes per group except *Pcm/Pcm* at 12 wks where $N = 2$.
[a] From the generalized estimating equations with correlations from repeated measures adjusted.

*Pcm* brain after 12 weeks of age appears less likely since excess peripheral iron is sequestered in RES macrophages and, hence, appears non-bioavailable, due to Hamp-mediated downregulation of Fpn1 (Mok et al., 2006). Indeed, brain iron content in aged *Pcm* heterozygous and homozygous animals was indistinguishable from wild-type controls (Mok et al., 2006) and there was no overt evidence of neurodegeneration (data not shown).

Due to the importance of iron homeostasis in mammalian development, perinatal iron deficiency has been extensively studied in rodents. These models vary in their methods to induce fetal iron deficiency and the length of postnatal dietary iron deficiency (Lozoff and Georgieff, 2006). In gestational/lactation models, pregnant dams are fed an iron-deficient diet starting around day 5 of gestation and continue an iron-deficient diet during lactation until weaning, at which point pups are fed a normal iron diet. This period of iron deficiency in rats is shorter than iron deficiency anemia observed in *Pcm* homozygotes. However, the correction to normal non-heme brain iron levels observed in 12-week-old *Pcm* homozygotes does not occur in iron-deficient rats (Felt and Lozoff, 1996). Thus, the *Pcm* mouse represents a powerful genetic model to study the regulatory mechanisms of brain iron uptake in response to developmental iron deficiency.

Within the retina, disruption of iron homeostasis can lead to cellular degeneration (He et al., 2007). At P0, the retina is still developing, with ongoing mitosis and lamination. The INBL includes post-mitotic ganglion, amacrine, horizontal cells, bipolar and Muller cell precursors (Cepko et al., 1996). Compared with wild-type control, Pcm retina at P0 displayed increased Fpn1 expression within the INBL, suggesting increased iron export in this location. Consistent with this, there was increased immunolabel for TfR1 in the Pcm retina at P0. This increase in TfR1 may be compensating for retinal iron deficiency caused by increased Fpn1 expression. While, *Pcm* homozygotes depicted no changes in retinal morphology or cell number in the ONL at this age (Fig. 4B), it is possible that developmental iron deficiency plays a role in the subsequent photoreceptor degeneration in older mice.

Interestingly, *Pcm* retinas exhibited an age-related degeneration that is significantly more severe than in wild-type controls (Fig. 4B, Table 1). As observed in this study, previous reports demonstrated that the retinas of wild-type A/J mice degenerate slowly with age (Danciger et al., 2003, 2007; Gresh et al., 2003). Intercrosses of albino and pigmented mouse strains identified quantitative trait loci (QTL) involved in age-related retinal degeneration in this inbred strain (Danciger et al., 2003, 2007). The QTLs mapped to several chromosomes and included *Antxr1*, *Ruvbl1*, and *Eefsec* (Danciger et al., 2007). Fpn1, which is located on chromosome 1 was not detected in this QTL screen and it remains to be determined whether Fpn1 interacts genetically with these loci. However, based on the progressive retinal phenotype in *Pcm* homozygotes, *Fpn1* appears to act as a genetic modifier of age-related retinal degeneration in this albino strain of mice.

In humans, retinopathy consisting of retinal hemorrhages and small nerve fiber layer infarcts (cotton-wool spots) are occasionally observed in cases of iron deficiency anemia (Carraro et al., 2001; Holt and Gordon-Smith, 1969). However, thinning of the ONL has not been described. In mice, mutation or disruption of genes integral to iron homeostasis often leads to anemia (Bernstein, 1987; Donovan et al., 2005; Trenor et al., 2000). Whereas retinal phenotypes might have generally been underreported, a subset of mouse mutants displays defects in this important compartment of the CNS. For example, Cp/Heph-deficient mice are anemic (Z. L. Harris and J. L. Dunaief, unpublished data) and display an age-related retinal degeneration. It is important to note Cp/Heph-deficient mice that survive to one year exhibit retinal iron accumulation in the RPE and widespread ONL thinning and RPE hypertrophy (Dunaief et al., 2005; Hadziahmetovic et al., 2008; Hahn et al., 2004). This represents a very different retinal phenotype compared with aged *Pcm* homozygotes, which are devoid of RPE hypertrophy or RPE iron accumulation. Thus whereas lack a functional iron export system systemically leads to an RPE iron overload in aged Cp/Heph-deficient mice, systemic dysregulation of the iron export protein Fpn1 in *Pcm* mice leads to slow, progressive ONL degeneration. Also supporting the importance of Fpn1 is RPE iron homeostasis is the observation that conditional disruption of *Fpn1* within the RPE leads to L-ferritin accumulation within Cre recombinase positive RPE and loss of the L-ferritin loaded RPE cells in aged mice (J. Iacovelli and J. L. Dunaief, unpublished data). Although changes in retinal iron levels could not be detected in *Pcm* retinas by L-ferritin IHC, Western analysis or tissue iron quantification, more subtle changes in retinal iron homeostasis may account for the degeneration seen in these retinas. The retinal phenotype bears striking similarities with spleen degeneration in *Pcm* embryos, wherein apoptotic cell death and spleen regression ensue in the context of elevated levels of Fpn1 expression (Mok et al., 2004b). Therefore, while the specific mechanism(s) of cellular degeneration await further investigation, this study demonstrates a novel function for Fpn1 in the regulation of long-term photoreceptor survival.

## 4. Experimental procedures

### 4.1. Mice and genotyping

This study employed *Pcm* mice on a fully congenic $N_{14}$ A/J background. Mice were fed a standard chow with an iron content of 240 ppm and genotyped as described previously (Mok et al., 2004a). Brains from wild-type and *Pcm* mutants were dissected at embryonic day 14.5 (E14.5), postnatal day 0 (P0), 3 and 12 weeks of age.

### 4.2. Iron determination

Non-heme iron in brain, retina, and retinal pigment epithelium/choroids was quantified based on the methodology of Torrance and Bothwell (1980). Samples were processed as described previously (Mok et al., 2004a). To determine the abundance and localization of iron in *Pcm* brain, Prussian blue staining of brain sections was accomplished using the Accustain iron staining kit (Sigma, St. Louis, MO), according to the manufacturer's protocol.

### 4.3. Histology, immunohistochemistry, and immunofluorescence

As described recently (Kim et al., 2007), dissected brains were fixed in Bouin's reagent, dehydrated in a graded series of ethanol, embedded in paraffin and sectioned midsagittally at 5-μm thickness. To allow for comparison of gross morphology and protein expression levels, sections from wild-type and *Pcm* homozygous brains were mounted side by side on the same slide. Sections were stained with hematoxylin and eosin (H and E) according to standard protocols and immunohistochemistry was performed as described previously (Mok et al., 2004b). For Fpn1, Dmt1 and TfR1 antigen retrieval, sections were boiled in 0.01 M citric acid, pH 6.0. Blocking was achieved with goat (Fpn1 and Dmt1) or horse serum (TfR1). Primary antibody incubations were performed overnight at 4°C using rabbit αFpn1 at 1:200 (Mok et al., 2006), rabbit αDmt1 at 1:100 (Alpha Diagnostic International) and mouse αTfR1 at 1:1000 dilution (Invitrogen). Secondary antibodies were peroxidase-conjugated with the Vectastain Elite ABC Kit (Vector Laboratories, Burlingame, CA) and antigen expression was detected with Vector NovaRED substrate (Vector Laboratories). Images were acquired with a Sony 085 CCD color RGB sensor digital camera mounted on a Zeiss Axioplan 2 microscope and processed with Adobe Photoshop software.

For immunofluorescence on P0 retina, pup heads were fixed in 4% parafomaldehyde in PBS and then cryoprotected in 30% Sucrose in PBS. Pup heads were embedded in Tissue-Tek OCT (Sakura Finetek, Torrance, CA). Immunofluorescence for Fpn1 and TfR1 was performed on 10 μm cryosections. For TfR1, antigen retrieval was performed as describe above prior to blocking. Sections were blocked as previously described (Dunaief et al., 2002) and incubated in rabbit αFpn1 (Mok et al., 2006) at a 1:100 dilution or rabbit αTfR1 at a 1:80 dilution. The secondary antibody used was donkey anti-rabbit-CY3 (Jackson ImmunoResearch Laboratories, West Grove, PA). Ommision of the primary antibody was used as a negative control. Sections were counterstained with Vectrashield containing DAPI (Vector Laboratories) and images were obtained using a Nikon epifluorescence microscope and Image Pro 6.0. Samples were processed in parallel and equivalent exposure times were used for all samples.

### 4.4. Morphologic analysis of the retina

Eyes were enucleated *post mortem* and fixed overnight in 2% gluteraldehyde/2% paraformaldehyde in PBS. Eyecups were prepared by removal of the anterior segment and embedded in JB-4 according to the manufacturer's protocol (Polysciences Inc., Warrington, PA). Semi-thin 3 μm section were cut and stained with Toluidine Blue O (Sigma). Images of sections containing optic nerve and separated by 30 μm were obtained for quantitative analysis using Nikon TE-300 epifluorescence microscope with Image Pro Plus 6.1 software (Media Cybernetics, Bethesda, MD). The number of photoreceptor nuclei per row present in the outer nuclear layer (ONL) was counted in three adjacent rows at a given distance from the optic nerve head. The average nuclei in the three adjacent rows was calculated from 5 sections from 3 eyes for each genotype at 7 wks and 1 yr and 2 eyes for each genotype at 12 wks. A *P*-value was generated using the generalized estimating equations with correlations from repeated measures applied. Differences of $P < 0.05$ were considered significant.

### 4.5. Western blot analysis

Brains were dissected from E14.5 embryos, P0 pups, as well as 3- and 12-week-old animals and were processed for Western blot analysis as described (Mok et al., 2004a). Briefly, following homogenization, brains were lysed in RIPA buffer plus Complete®, EDTA-free protease inhibitor (Roche), extract supernatant was collected and protein was quantified using the Bio-Rad *DC* Protein Assay kit (Bio-Rad). Fifty micrograms of total protein were mixed with equal volume sample buffer with β-mercaptoethanol. For detection of Dmt1, TfR1 and actin expression, samples were boiled; non-heated samples were employed for Fpn1 analysis. Protein lysates were separated on 8% SDS-PAGE and transferred to PVDF membrane. Blocking was achieved by incubation in TRIS-buffered saline containing 5% milk and 0.1% Tween 20. Membranes were incubated overnight at 4 °C with the following primary antibodies: rabbit α-Fpn1 at 1:1000 dilution (Mok et al., 2004a), rabbit α-Dmt1 at 1:2000 (Alpha Diagnostic International), mouse α-TfR1 at 1:2000 (Invitrogen, Carlsbad, CA) and goat α-actin at 1:5000 (Santa Cruz Biotechnology, Santa Cruz, CA). Following washes, membranes were incubated with horseradish peroxidase-conjugated secondary antibodies (1:10 000 dilution) and signals were developed using ECL reagent (Santa Cruz Biotechnology).

### 4.6. Quantitative real-time RT-PCR

Total RNA was extracted from P0 or 12-week-old wild-type and *Pcm* brain using Trizol reagent (Invitrogen). First-strand

synthesis from 50 to 600 ng of total RNA employed Superscript III RTase (Invitrogen) with random hexamers. PCR was performed using the 2×TaqMan® Universal Master Mix, no UNG (Applied Biosystems) and the 7500 Fast System (Applied Biosystems) according to the manufacturer's protocol. The following Taqman MGB probes from Applied Biosystems were employed: *Fpn1* (exon junction 3–4, Mm00489837_m1), *TfR1* (exon junction 2–3, Mm00441941_m1), *Trf* (exon junction 1–2, Mm00446708_m1), *Dmt1* (exon junction 15–16, Mm00435363_m1), *Hamp* (exon junction 1–2, Mm00519025_m1) and *18S* ribosomal RNA (4319413E) as an endogenous control for each sample. The relative levels of mRNA expression were expressed as a ratio of the gene-specific probe to *18S* rRNA and normalized to a single wild-type ratio set to 1.

## REFERENCES


Aisen, P., Enns, C., Wessling-Resnick, M., 2001. Chemistry and biology of eukaryotic iron metabolism. Int. J. Biochem. Cell. Biol. 33, 940–959.

Ballabh, P., Braun, A., Nedergaard, M, 2004. The blood–brain barrier: an overview: structure, regulation, and clinical implications. Neurobiol. Dis. 16, 1–13.

Beard, J., 2003. Iron deficiency alters brain development and functioning. J. Nutr. 133, 1468S–1472S.

Beard, J., 2007. Recent evidence from human and animal studies regarding iron status and infant development. J. Nutr. 137, 524S–530S.

Beard, J.L., Connor, J.R., 2003. Iron status and neural functioning. Annu. Rev. Nutr. 23, 41–58.

Bernstein, S.E., 1987. Hereditary hypotransferrinemia with hemosiderosis, a murine disorder resembling human atransferrinemia. J. Lab. Clin. Med. 110, 690–705.

Bradbury, M.W., 1997. Transport of iron in the blood–brain–cerebrospinal fluid system. J. Neurochem. 69, 443–454.

Carraro, M.C., Rossetti, L., Gerli, G.C., 2001. Prevalence of retinopathy in patients with anemia or thrombocytopenia. Eur. J. Haematol. 67, 238–244.

Cepko, C.L., Austin, C.P., Yang, X., Alexiades, M., Ezzeddine, D., 1996. Cell fate determination in the vertebrate retina. Proc. Natl. Acad. Sci. U. S. A. 93, 589–595.

Curtis, A.R., Fey, C., Morris, C.M., Bindoff, L.A., Ince, P.G., Chinnery, P.F., Coulthard, A., Jackson, M.J., Jackson, A.P., McHale, D.P., Hay, D., Barker, W.A., Markham, A.F., Bates, D., Curtis, A., Burn, J., 2001. Mutation in the gene encoding ferritin light polypeptide causes dominant adult-onset basal ganglia disease. Nat. Genet. 28, 350–354.

Danciger, M., Lyon, J., Worrill, D., LaVail, M.M., Yang, H., 2003. A strong and highly significant QTL on chromosome 6 that protects the mouse from age-related retinal degeneration. Invest. Ophthalmol. Vis. Sci. 44, 2442–2449.

Danciger, M., Yang, H., Ralston, R., Liu, Y., Matthes, M.T., Peirce, J., Lavail, M.M., 2007. Quantitative genetics of age-related retinal degeneration: a second F1 intercross between the A/J and C57BL/6 strains. Mol. Vis. 13, 79–85.

Dentchev, T., Hahn, P., Dunaief, J.L., 2005. Strong labeling for iron and the iron-handling proteins ferritin and ferroportin in the photoreceptor layer in age-related macular degeneration. Arch. Ophthalmol. 123, 1745–1746.

Donovan, A., Lima, C.A., Pinkus, J.L., Pinkus, G.S., Zon, L.I., Robine, S., Andrews, N.C., 2005. The iron exporter ferroportin/Slc40a1 is essential for iron homeostasis. Cell. Metab. 1, 191–200.

Dunaief, J.L., King, A., Esumi, N., Eagen, M., Dentchev, T., Sung, C.H., Chen, S., Zack, D.J., 2002. Protein Phosphatase 1 binds strongly to the retinoblastoma protein but not to p107 or p130 in vitro and in vivo. Curr. Eye Res. 24, 392–396.

Dunaief, J.L., Richa, C., Franks, E.P., Schultze, R.L., Aleman, T.S., Schenck, J.F., Zimmerman, E.A., Brooks, D.G., 2005. Macular degeneration in a patient with aceruloplasminemia, a disease associated with retinal iron overload. Ophthalmology 112, 1062–1065.

Felt, B.T., Lozoff, B., 1996. Brain iron and behavior of rats are not normalized by treatment of iron deficiency anemia during early development. J. Nutr. 126, 693–701.

Gresh, J., Goletz, P.W., Crouch, R.K., Rohrer, B., 2003. Structure–function analysis of rods and cones in juvenile, adult, and aged C57bl/6 and Balb/c mice. Vis. Neurosci. 20, 211–220.

Hadziahmetovic, M., Dentchev, T., Song, Y., Haddad, N., He, X., Hahn, P., Pratico, D., Wen, R., Harris, Z.L., Lambris, J.D., Beard, J., Dunaief, J.L., 2008. Ceruloplasmin/hephaestin knockout mice model morphologic and molecular features of AMD. Invest. Ophthalmol. Vis. Sci. 49, 2728–2736.

Hahn, P., Milam, A.H., Dunaief, J.L., 2003. Maculas affected by age-related macular degeneration contain increased chelatable iron in the retinal pigment epithelium and Bruch's membrane. Arch. Ophthalmol. 121, 1099–1105.

Hahn, P., Qian, Y., Dentchev, T., Chen, L., Beard, J., Harris, Z.L., Dunaief, J.L., 2004. Disruption of ceruloplasmin and hephaestin in mice causes retinal iron overload and retinal degeneration with features of age-related macular degeneration. Proc. Natl. Acad. Sci. U. S. A. 101, 13850–13855.

Hentze, M.W., Muckenthaler, M.U., Andrews, N.C., 2004. Balancing acts: molecular control of mammalian iron metabolism. Cell 117, 285–297.

He, X., Hahn, P., Iacovelli, J., Wong, R., King, C., Bhisitkul, R., Massaro-Giordano, M., Dunaief, J.L., 2007. Iron homeostasis and toxicity in retinal degeneration. Prog. Retin. Eye Res. 26, 649–673.

Holt, J.M., Gordon-Smith, E.C., 1969. Retinal abnormalities in diseases of the blood. Br. J. Ophthalmol. 53, 145–160.

Jeong, S.Y., David, S., 2003. Glycosylphosphatidylinositol-anchored ceruloplasmin is required for iron efflux from cells in the central nervous system. J. Biol. Chem. 278, 27144–27148.

Jeong, S.Y., David, S., 2006. Age-related changes in iron homeostasis and cell death in the cerebellum of ceruloplasmin-deficient mice. J. Neurosci. 26, 9810–9819.

Kim, S.Y., Levenson, J.M., Korsmeyer, S., Sweatt, J.D., Schumacher, A., 2007. Developmental regulation of Eed complex composition governs a switch in global histone modification in brain. J. Biol. Chem. 282, 9962–9972.

Kwik-Uribe, C.L., Gietzen, D., German, J.B., Golub, M.S., Keen, C.L., 2000. Chronic marginal iron intakes during early development in mice result in persistent changes in dopamine metabolism and myelin composition. J. Nutr. 130, 2821–2830.

LaVaute, T., Smith, S., Cooperman, S., Iwai, K., Land, W., Meyron-Holtz, E., Drake, S.K., Miller, G., Abu-Asab, M., Tsokos, M., Switzer 3rd, R., Grinberg, A., Love, P., Tresser, N., Rouault, T.A., 2001. Targeted deletion of the gene encoding iron regulatory protein-2 causes misregulation of iron metabolism and neurodegenerative disease in mice. Nat. Genet. 27, 209–214.

Lozoff, B., Georgieff, M.K., 2006. Iron deficiency and brain development. Semin Pediatr. Neurol. 13, 158–165.

Miyajima, H., Nishimura, Y., Mizoguchi, K., Sakamoto, M., Shimizu, T., Honda, N., 1987. Familial apoceruloplasmin deficiency associated with blepharospasm and retinal degeneration. Neurology 37, 761–767.

Mok, H., Jelinek, J., Pai, S., Cattanach, B.M., Prchal, J.T., Youssoufian, H., Schumacher, A., 2004a. Disruption of ferroportin 1 regulation causes dynamic alterations in iron

homeostasis and erythropoiesis in polycythaemia mice. Development 131, 1859–1868.
Mok, H., Mendoza, M., Prchal, J.T., Balogh, P., Schumacher, A., 2004b. Dysregulation of ferroportin 1 interferes with spleen organogenesis in polycythaemia mice. Development 131, 4871–4881.
Mok, H., Mlodnicka, A.E., Hentze, M.W., Muckenthaler, M., Schumacher, A., 2006. The molecular circuitry regulating the switch between iron deficiency and overload in mice. J. Biol. Chem. 281, 7946–7951.
Moos, T., Morgan, E.H., 2000. Transferrin and transferrin receptor function in brain barrier systems. Cell. Mol. Neurobiol. 20, 77–95.
Morita, H., Ikeda, S., Yamamoto, K., Morita, S., Yoshida, K., Nomoto, S., Kato, M., Yanagisawa, N., 1995. Hereditary ceruloplasmin deficiency with hemosiderosis: a clinicopathological study of a Japanese family. Ann. Neurol. 37, 646–656.
Nemeth, E., Tuttle, M.S., Powelson, J., Vaughn, M.B., Donovan, A., Ward, D.M., Ganz, T., Kaplan, J., 2004. Hepcidin regulates cellular iron efflux by binding to ferroportin and inducing its internalization. Science 306, 2090–2093.
Pandolfo, M., 1999. Friedreich's ataxia: clinical aspects and pathogenesis. Semin. Neurol. 19, 311–321.
Patel, B.N., Dunn, R.J., Jeong, S.Y., Zhu, Q., Julien, J.P., David, S., 2002. Ceruloplasmin regulates iron levels in the CNS and prevents free radical injury. J. Neurosci. 22, 6578–6586.
Ponka, P., 2004. Hereditary causes of disturbed iron homeostasis in the central nervous system. Ann. N.Y. Acad. Sci. 1012, 267–281.
Rouault, T.A., 2001. Systemic iron metabolism: a review and implications for brain iron metabolism. Pediatr. Neurol. 25, 130–137.
Taneja, V., Mishra, K., Agarwal, K.N., 1986. Effect of early iron deficiency in rat on the gamma-aminobutyric acid shunt in brain. J. Neurochem. 46, 1670–1674.
Taylor, E.M., Crowe, A., Morgan, E.H., 1991. Transferrin and iron uptake by the brain: effects of altered iron status. J. Neurochem. 57, 1584–1592.
Trenor III, C.C., Campagna, D.R., Sellers, V.M., Andrews, N.C., Fleming, M.D., 2000. The molecular defect in hypotransferrinemic mice. Blood 96, 1113–1118.
Wu, L.J., Leenders, A.G., Cooperman, S., Meyron-Holtz, E., Smith, S., Land, W., Tsai, R.Y., Berger, U.V., Sheng, Z.H., Rouault, T.A., 2004. Expression of the iron transporter ferroportin in synaptic vesicles and the blood–brain barrier. Brain Res. 1001, 108–117.
Xu, X., Pin, S., Gathinji, M., Fuchs, R., Harris, Z.L., 2004. Aceruloplasminemia: an inherited neurodegenerative disease with impairment of iron homeostasis. Ann. N.Y. Acad. Sci. 1012, 299–305.
Yamaguchi, K., Takahashi, S., Kawanami, T., Kato, T., Sasaki, H., 1998. Retinal degeneration in hereditary ceruloplasmin deficiency. Ophthalmologica 212, 11–14.
Yehuda, S., Youdim, M.B., 1989. Brain iron: a lesson from animal models. Am. J. Clin. Nutr. 50, 618–625 discussion 625–9.
Zhou, B., Westaway, S.K., Levinson, B., Johnson, M.A., Gitschier, J., Hayflick, S.J., 2001. A novel pantothenate kinase gene (PANK2) is defective in Hallervorden–Spatz syndrome. Nat. Genet. 28, 345–349.